Radar reflectivity calibration using differential propagation phase measurement

J. Vivekanandan,[1] Guifu Zhang,[1] Scott M. Ellis,[1] D. Rajopadhyaya,[2] and Susan K. Avery[2]

Received 11 March 2002; revised 5 June 2002; accepted 12 June 2002; published 12 March 2003.

[1] A method for calibrating radar reflectivity using polarization radar measurements in rain is described. Accurate calibration of radar reflectivity is essential for obtaining reliable rain rate estimation. In the case of polarization radar, rain rate can be independently estimated using power and phase measurements. Thus phase measurement can be estimated from power measurements. Comparison of the direct estimate of propagation phase (Φ^m) measurement, which is unaffected by absolute calibration of the radar system, with the estimated propagation phase (Φ^e) from power measurements is the basis for the calibration method. Polarization measurements such as reflectivity (Z), differential reflectivity (Z_{DR}), and differential propagation phase (Φ_{DP}) are sensitive to drop size distribution (DSD) and mean drop shape. It is important to devise a calibration technique relatively unperturbed by changes in DSD and drop shape. Statistical fluctuation in Φ^e is derived to estimate the accuracy of the calibration procedure, raindrop shape, and attenuation. The proposed method is applied for calibrating reflectivity measurements of the National Center for Atmospheric Research (NCAR) S-band polarization radar (S-Pol) in midlatitude, subtropical, and tropical rain events. *INDEX TERMS:* 3354 Meteorology and Atmospheric Dynamics: Precipitation (1854); 3360 Meteorology and Atmospheric Dynamics: Remote sensing; 3394 Meteorology and Atmospheric Dynamics: Instruments and techniques; 6904 Radio Science: Atmospheric propagation; 6969 Radio Science: Remote sensing; *KEYWORDS:* polarization radar calibration, reflectivity, differential reflectivity, differential phase, raindrop size distribution

Citation: Vivekanandan, J., G. Zhang, S. M. Ellis, D. Rajopadhyaya, and S. K. Avery, Radar reflectivity calibration using differential propagation phase measurement, *Radio Sci.*, *38*(3), 8049, doi:10.1029/2002RS002676, 2003.

1. Introduction

[2] Bias in reflectivity (Z) introduces bias in Z-based rain rate (R) estimates and the amount of the bias is a function of the particular Z-R relation. In the case of the NEXRAD (Next Generation Weather Radar) Z-R relation, 1 dB bias in reflectivity produces 18% bias in radar-based rain rate estimation. Thus, unbiased reflectivity measurements are essential for reliable radar-based estimates. Absolute calibration of radar reflectivity depends on both transmitter and receiver characteristics. Even with a perfect system calibration, measured reflectivity might be biased by the actual reflectivity gradient in the radar resolution volume, antenna side lobes, atmospheric absorption and attenuation due to the precipitation. In this paper, only the bias due to the transmitter and receiver chain is studied.

[3] Reflectivity can be calibrated using a known signal source such as transmit power from a horn antenna in the far zone or the solar radiation. When a known external signal source is used, the radar does not transmit, and only the receiver system is calibrated. In the case of solar calibration, the receiver should be sensitive enough to detect the low signal power (−100 dBm). Also, the main lobe beam width should be less than 0.5° for satisfying the beam-filled condition. In the transmit and receive mode, a highly reflective test sphere suspended from a tethered balloon can be used as a known reference target for calibration. But the sphere being a point target does not fill the radar beam; as a result, only the on-axis gain of the beam is measured.

[4] Self-consistency among reflectivity, differential reflectivity and propagation phase [*Scarchilli et al.*,

[1]National Center for Atmospheric Research, Boulder, Colorado, USA.
[2]Cooperative Institute for Research in Environmental Sciences, University of Colorado, Boulder, Colorado, USA.

0048-6604/03/2002RS002676$11.00

1996] can be used for calibrating the radar system [*Goddard et al.*, 1994]. One of the advantages of using power and phase measurements from a single radar is the elimination of sampling volume differences among the measurements. Comparison between rain gauge observation and radar-based rain estimation is also used for inferring the reflectivity bias [*Brandes et al.*, 1999]. However, nonlinearity in the *Z*-R relation, and sampling volume mismatch between radar and rain gauge observation requires averaging over considerable spatial and temporal scales in order to obtain reliable estimates. In the case of polarization radar, rain rate can be independently estimated using the power measurements (Z and Z_{DR}) and phase measurements (K_{DP}) [*Gorgucci et al.*, 1992] and hence conceptually, phase measurement can be estimated from power measurements [*Gorgucci et al.*, 1999a, 1999b]. *Zrnic and Ryzhkov* [1996] and *Vivekanandan et al.* [1999] show the specific propagation phase is not affected by the absolute calibration of the radar system, attenuation and partial beam blockage. Recent results show that K_{DP} can be derived from the Z and Z_{DR} observations [*Gorgucci et al.*, 1993, 1999a, 1999b; *Goddard et al.*, 1994]. Thus, in principle, polarization radar measurements in rain, particularly in the propagation phase, can be used for calibrating the reflectivity.

[5] The proposed method using polarization measurements for calibrating reflectivity should be carefully evaluated because the accuracy of the calibration is susceptible to variation in the following: (1) raindrop size distribution and mean raindrop shape distribution, (2) attenuation due to precipitation and gaseous absorption, and (3) statistical fluctuation in estimated and measured K_{DP} (or range integrated K_{DP}, i.e., Φ_{DP}). A description of the relation between K_{DP} and power measurements (Z and Z_{DR}) and its variation due to the changes in drop size and shape distributions is presented in section 2. Signal statistics simulations and estimated accuracies in measured and estimated Φ_{DP} are described in section 3. A procedure for performing the absolute calibration is outlined in section 4. The results of the radar calibration in the midlatitudes (Kansas), subtropics (Florida) and the tropics (Brazil) are discussed in section 5. Finally, the paper ends with a summary and conclusions in section 6.

2. Self-Consistency Among Z, Z_{DR}, and K_{DP}

2.1. Description of Polarization Observables

[6] Polarization radar observables depend on the microphysical characteristics of raindrops; namely, particle size, shape and orientation relative to the local vertical direction [*McCormick and Hendry*, 1975]. The backscattered power is proportional to the incoherent sum of the power backscattered by each particle in the radar resolution volume. The advent of pulse-to-pulse switching between horizontal (h) and vertical (v) polarization for transmit states and reception of the associated co and cross-polarized returned signals has augmented the accuracy of precipitation medium characterization [*Bringi and Hendry*, 1990]. The ability of polarization radars to obtain differential propagation phase and differential reflectivity is a major advantage over traditional reflectivity observations. Reflectivity (Z_{hh}) is related to the horizontally polarized power backscattered from a horizontally polarized transmitted wave (i.e., copolar return). Reflectivity is the sixth moment of the particle size distribution when particle size is small compared to the wavelength. Differential reflectivity (Z_{DR}) is the ratio of the horizontal power received from a horizontally transmitted wave (hh) to the vertical power received from a vertically transmitted wave (vv) and can be interpreted as the reflectivity weighted mean axis ratio of the raindrops in the radar resolution volume [*Jameson*, 1983a, 1983b]. The differential propagation phase constant (K_{DP}) is the specific propagation phase between the two polarization states experienced by the forward traveling wave. Z_{hh}, and Z_{DR} are expressed in $mm^6\ m^{-3}$ and logarithmic units (dB), respectively, while K_{DP} is expressed in terms of degrees per kilometer.

[7] Polarization radar observables such as horizontal reflectivity (Z_{hh}), vertical reflectivity (Z_{vv}) and Z_{DR} for an ensemble of particles are as follows:

$$Z_{hh,vv} = \frac{4\lambda^4}{\pi^4 |K_w|^2} \int_{D_{min}}^{D_{max}} \left| f_{hh,vv}(D) \right|^2 N(D) dD \quad \left[mm^6\ m^{-3}\right] \tag{1}$$

$$Z_{DR} = 10 \log\left(\frac{Z_{hh}}{Z_{vv}}\right) \quad [dB] \tag{2}$$

where $f_{hh,vv}$ are the elements of the backscattering matrix [*Vivekanandan et al.*, 1991], K_w is the dielectric factor of the droplet, λ is the wavelength, D is the equivalent spherical diameter and N(D) is the particle size distribution.

[8] The scattering process in a precipitation medium can be approximated by first order multiple scattering [*Oguchi*, 1983]. Under such conditions, the backscattered signal received by the radar has both the range cumulative forward scattering and the gate-by-gate backscattering characteristics of the ensemble of scatterers in the medium. Range cumulative attenuation and propagation phase of an ensemble of scatterers can be recovered from backscattered signals [*Jameson and Meuller*, 1985]. The specific differential propagation phase (K_{DP}), the attenuation of horizontally polarized

wave (A_{hh}) and the differential attenuation (A_{DP}) are defined as:

$$K_{DP} = \frac{180\lambda}{\pi} \int_{D_{min}}^{D_{max}} \mathrm{Re}[f_{hh}(0,D) - f_{vv}(0,D)]N(D)dD \quad \left[\mathrm{deg\ km^{-1}}\right] \tag{3}$$

$$A_H = 8.686\lambda \int_{D_{min}}^{D_{max}} \mathrm{Im}[f_{hh}(0,D)]N(D)dD \quad \left[\mathrm{dB\ km^{-1}}\right] \tag{4}$$

$$A_{DP} = 8.686\lambda \int_{D_{min}}^{D_{max}} \mathrm{Im}[f_{hh}(0,D) - f_{vv}(0,D)]N(D)dD \quad \left[\mathrm{dB\ km^{-1}}\right] \tag{5}$$

where $f_{hh,vv}(0, D)$ are the forward scattering amplitudes, the argument 0 in scattering amplitude corresponds to the angle between incident and scattered directions and λ is the wavelength. The two-way differential propagation phase (Φ_{DP}) between two range locations r_1 and r_2 is defined as:

$$\Phi_{DP} = 2\int_{r_1}^{r_2} K_{DP}(r)dr \quad [\mathrm{degrees}]. \tag{6}$$

[9] For a specified drop size distribution, raindrop shape, and canting angle, the above described polarization parameters, namely, Z or Z_{hh}, Z_{DR} and K_{DP} can be calculated using the scattering amplitudes [*Vivekanandan et al.*, 1991]. To simplify the notation, in this paper Z represents Z_{hh}. The model based polarization parameters can be analyzed to obtain a relation between propagation phase (K_{DP}) and power (Z and Z_{DR}) parameters that can be used for calibrating reflectivity.

[10] Disdrometer and particle measuring probe measurements of raindrop size distribution show that a Gamma function adequately represents the natural variation in drop size distribution (DSD). The Gamma function form of N(D) is

$$N(D) = N_0 D^{\mu} e^{-\Lambda D} \tag{7}$$

where $N_0\Lambda^{-(\mu+1)}\Gamma(\mu + 1)$ is the raindrop concentration, μ and Λ represents the shape and slope factors of the size distribution and the D drop in diameter. The median volume diameter D_0 is a function of μ and Λ [*Ulbrich*, 1983] as,

$$D_0 = \frac{3.67 + \mu}{\Lambda}. \tag{8}$$

Most of the polarization model calculations shown in earlier studies used the range of N_0, D_0 and μ based on the work of *Ulbrich* [1983]. *Haddad et al.* [1997] describe a method for simulating parameters of Gamma distribution where the parameters (μ and N_0) are independent of each other. The method makes use of observed DSDs near Darwin, Australia during the summer seasons of 1988–1990. Simulated DSDs using the work of *Haddad et al.* [1997] with equilibrium raindrop shape are used for calculating polarization observables. The mean and standard deviation of canting angle are assumed to be 2° and 5° respectively.

[11] Figure 1a shows the scatterplots of simulated K_{DP} versus estimated K_{DP} from Z and Z_{DR}. A power law fit is used for obtaining a relation between phase and power observables. The model calculations show that K_{DP} can be obtained using Z and Z_{DR} as,

$$K_{DP} = 2.79 \times 10^{-5} Z^{1.0086} Z_{DR}^{-0.9543}. \tag{9}$$

In the above equation, Z is in mm^6/m^3, Z_{DR} is in linear units and K_{DP} in deg km^{-1}. The above equation relating phase and power is the basis for reflectivity calibration. Since K_{DP} is linearly proportional to Z (in mm^6/m^3), the reflectivity bias can be estimated from the ratio between the estimated and measured Φ_{DP}.

[12] Using the same set of simulated data, attenuation at horizontal polarization and differential attenuation versus K_{DP} is also studied. Figures 1b and 1c show scatterplots between A_H and A_{DP} versus K_{DP} for the simulated data set. The best fit lines for attenuation (A_H) and differential attenuation (A_{DP}) in dB km^{-1} versus K_{DP} are:

$$A_H = 0.017K_{DP} \tag{10}$$

$$A_{DP} = 0.0037K_{DP}. \tag{11}$$

[13] The following sections describe the sensitivity of equations (9), (10), and (11), to microphysical variations in raindrop size and shape distributions. Hereafter, the above three equations will be referred to as the calibration equations. The attenuation equation is in good agreement with *Bringi et al.* [1990] and the relation between K_{DP} and power measurements is also similar to

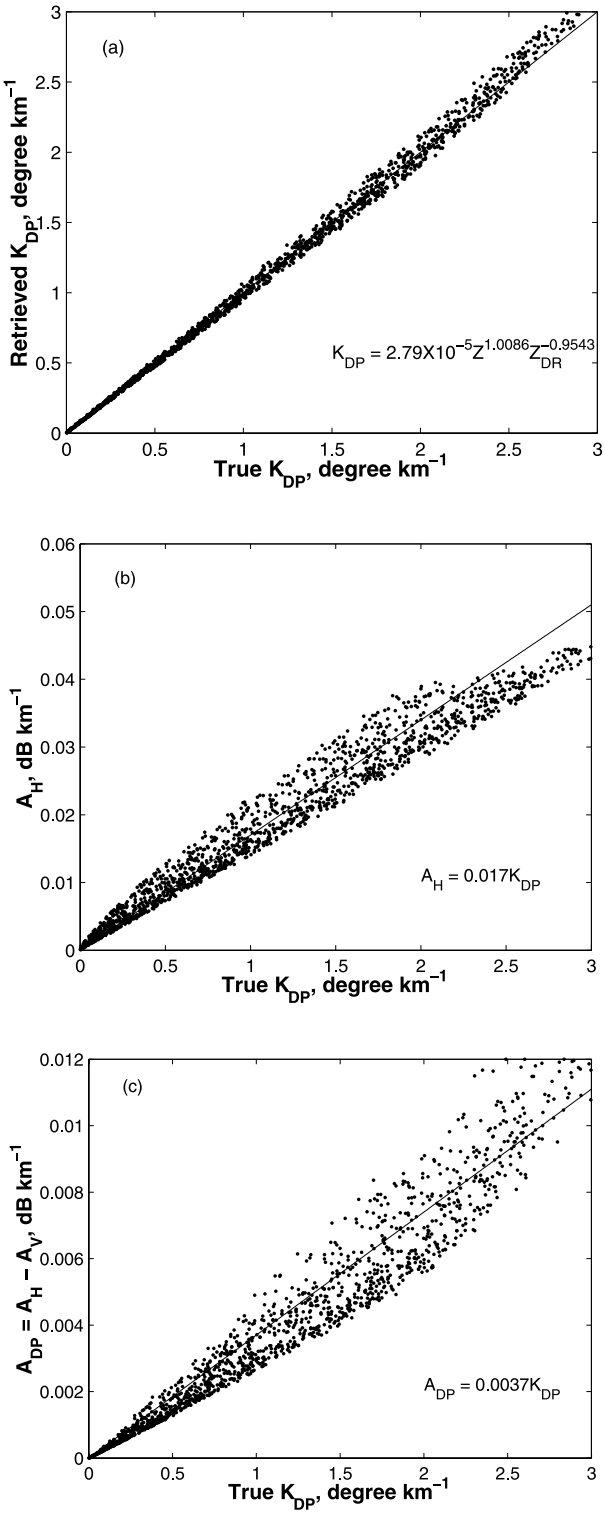

Figure 1. (opposite) (a) Estimated K_{DP} from power measurements (Z and Z_{DR}) versus true K_{DP} for Gamma drop size distribution (DSD). Raindrop shape is assumed equilibrium. (b) Specific attenuation versus K_{DP} for Gamma drop size distribution (DSD). Raindrop shape is assumed equilibrium. (c) Differential attenuation versus K_{DP} for Gamma drop size distribution (DSD). Raindrop shape is assumed equilibrium.

the corresponding equation by *Gorgucci et al.* [1999a, 1999b].

2.2. Drop Size Distribution

[14] As discussed in the previous section, most of the polarization model calculations shown in the earlier studies used the range of N_0, D_0 and μ based on the work of *Ulbrich* [1983]. The Gamma DSD with three parameters (N_0, μ, and Λ) is capable of describing a broader variation in raindrop size distribution than an exponential distribution which is a special case of Gamma distribution with $\mu = 0$. It has been found that the three parameters are not mutually independent [*Ulbrich*, 1983; *Haddad et al.*, 1997]. *Haddad et al.* [1997] parameterized rain DSD with an equivalent set of transformed parameters that are uniformly random. The effort has concentrated on generating Gamma DSDs from independent random variables.

[15] The three DSD parameters are not physical parameters such as liquid water content or median volume diameter, hence various normalization techniques are used [*Willis*, 1984; *Testud et al.*, 2001]. Since the dimension of N_0 is ill defined, *Chandrasekar and Bringi* [1987] proposed to use the total number concentration N_t instead of N_0. Furthermore, a normalized Gamma distribution was first proposed by Willis and recently adopted by Illingworth and Blackman to eliminate the dependence between N_0 and μ [*Willis*, 1984; *Illingworth and Blackman*, 1999]. They recommended using physically meaningful parameters to characterize a Gamma DSD. Nevertheless, the number of parameters is the same, and the DSD expression becomes more complicated. In practice, there is no simplification of the DSD function except that the DSD parameters are expressed using N_T, LWC, and D_0.

[16] During a recent analysis of data measured by a video-disdrometer [*Schonhuber et al.*, 1997], it was found there is a high correlation between the shape (μ) and slope (Λ) parameters. The fitted μ-Λ relation from the video-disdrometer measurements collected during a special field experiment in east-central Florida was used to evaluate the potential for polarization radar to estimate rainfall in a subtropical environment. The μ-Λ relation is also in good agreement with a number of earlier studies

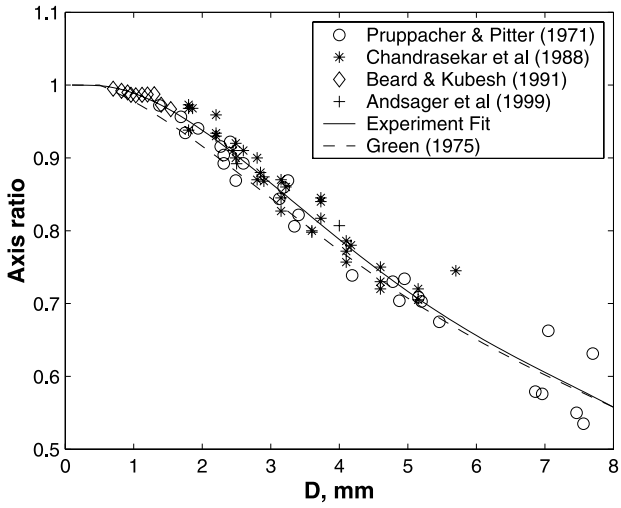

Figure 2. Scatter plot of five different drop axis ratios published by various investigators as a function of raindrop size. Equilibrium axis ratio [*Green*, 1975] and the proposed axis ratio plotted are as a function of the equivolume drop diameter.

that reported Gamma DSD parameters for convective and stratiform precipitation in various parts of the world [*Zhang et al.*, 2001].

[17] The relation between μ and Λ, derived from disdrometer observations, reduces three parameter Gamma DSDs into a constrained Gamma DSD. Since the constrained Gamma DSD has only two independent parameters, it can be directly estimated using Z and Z_{DR}. The advantage of constrained Gamma DSD is a closed-form and physically based calibration equation and the resultant expression may be much more general than a power law fit derived using a discrete set of random variations in DSD parameters. Again assuming an equilibrium drop shape, mean and standard deviation of canting angle as 2° and 5° respectively, the following set of calibration equations is derived:

$$K_{DP} = 5.97 \times 10^{-5} Z Z_{\mathrm{DR}}^{-2.76} \tag{12}$$

$$A_H = 0.017 K_{DP} \tag{13}$$

$$A_{DP} = 0.0036 K_{DP}. \tag{14}$$

The attenuation and differential attenuation equations are similar for both discrete and μ-Λ relation-based constrained DSDs. Both equations (9) and (12) are linear in Z and estimated $\mathrm{K_{DP}}$ is comparable for a specified set of Z and Z_{DR}. Thus the closed-form calibration equation based on the μ-Λ relation represents the detailed simulation based on a discrete form of DSD. In the next section, the calibration equation is derived for constrained Gamma DSD with nonequilibrium mean drop shape to study the sensitivity to drop shape on the calibration equation.

2.3. Raindrop Shape

[18] Even though the μ-Λ relation simplifies the DSD representation, any difference between assumed and actual microphysical parameters such as shape and canting angle might introduce significant uncertainties in polarization radar-based retrieval. Equilibrium shape of raindrops is assumed in the previous section while some observations suggested that a more spherical shape should be adapted [*Goddard and Cherry*, 1984]. Equilibrium shape of raindrops is assumed for maintaining continuity with earlier studies [*Bringi and Hendry*, 1990 and the references therein]. There has been considerable discussion about the deviation of the drop axis ratio from its equilibrium value [*Chandrasekar et al.*, 1988; *Beard and Kubesh*, 1991; *Bringi et al.*, 1998, *Beard and Chuang*, 1987; *Andsager et al.*, 1999]. Figure 2 shows a plot of three different drop axis ratio measurements published by various investigators as a function of raindrop size. It is interesting to note that each of the investigators analyzed only a discrete number of raindrop sizes. The equilibrium axis ratio proposed by *Green* [1975] is shown as a dashed line.

[19] The work of *Chandrasekar et al.* [1988] is derived from instrumented aircraft observations and shows that axis ratios of 3–4 mm size drops are in equilibrium. They argue that the concurrence of their results with the equilibrium axis ratios is due to suppression of oscillations by ice cores in partially melted raindrops. A laboratory study shows that the average axis ratio of 1.0–1.5 mm is more spherical than the equilibrium value [*Beard and Kubesh*, 1991]. Thus, there are a number of recent studies on raindrop shape that can be used for obtaining a shape versus size relationship for the entire drop diameter range. We fitted a smooth curve that optimally describes the results by *Pruppucher and Pitter* [1971], *Chandrasekar et al.* [1988], and *Beard and Kubesh* [1991]. We extended the results to smaller diameters with a smooth polynomial. The polynomial fit is made by assuming that the drop axis ratio merges smoothly with the equilibrium axis ratio in the higher diameter regime. The proposed polynomial fit can be represented as,

$$r = 0.9951 + 0.02510D - 0.03644D^2 + 0.005030D^3 - 0.0002492D^4 \tag{15}$$

where r is the drop axis ratio and D is the equivolume drop diameter measured in mm. The solid line in Figure 2

shows the proposed axis ratio plotted as a function of the equivolume drop diameter, which is more spherical than the equilibrium shape.

[20] The impact of slight deviations in shape from the equilibrium axis ratio on K_{DP} and Z_{DR} is not fully resolved because polarization radar observations are sensitive to both drop size distribution and raindrop shape. In practice, techniques that depend on both K_{DP} and Z_{DR} are relatively insensitive to the precise form of the axis ratio and size distribution [*Zrnic and Ryzhkov*, 1996]. In the case of constrained Gamma DSD with the proposed mean axis ratio, the set of calibration equations are:

$$K_{DP} = 3.32 \times 10^{-5} Z Z_{DR}^{-2.05} \tag{16}$$

$$A_H = 0.02 K_{DP} \tag{17}$$

$$A_{DP} = 0.0038 K_{DP}. \tag{18}$$

[21] In the case of proposed raindrop shape, median size raindrops are less oblate than in the case of equilibrium axis ratio and hence, for a specified rainrate, the corresponding Z_{DR} and K_{DP} are smaller. Comparing the above equations with the equations based on equilibrium axis ratio, the estimated K_{DP} for a specified Z and Z_{DR} is lower by 30%, but the attenuation for a given K_{DP} is higher. However, the estimated K_{DP} using the attenuation corrected Z and Z_{DR} is within 15% of the corresponding estimate based on equilibrium raindrop shape. Thus, it is important to use the corresponding pair of K_{DP}, A_H, and A_{DP} best fit lines that are derived for specified DSD and drop shape.

[22] In a precipitation free region, attenuation due to atmospheric gases, namely oxygen and water vapor, should be considered. The gaseous attenuation is directly proportional to distance traversed by the radar beam in the troposphere. For a standard atmosphere, two-way gaseous absorption is 1.5 dB for 50 km range [*Doviak and Zrnic*, 1993]. The magnitude of attenuation is comparable to the accuracy in reflectivity measurement. Hence, it is important to account for gaseous attenuation when estimating reflectivity bias.

3. Statistical Fluctuation in Estimation of Φ_{DP} Using Z and Z_{DR}

[23] As shown in the previous section, for a given Z and Z_{DR}, K_{DP} can be estimated. The measured K_{DP} is estimated as the slope of the range profile of measured Φ_{DP} (Φ^m). In the case of precipitation gradient or nonuniform precipitation, K_{DP} may not be uniform in the path over which K_{DP} is estimated and hence only a mean value of K_{DP} over a spatial scale of 2 to 5 km is valid. Thus it is difficult to compare the point estimate of K_{DP} derived from Z and Z_{DR} because K_{DP} estimated from Φ_{DP} is a range averaged parameter. Estimated K_{DP} can be summed as a function of range to estimate Φ_{DP} (Φ^e). Then an identical least squares fit can be performed on measured and estimated Φ_{DP} for minimizing the effect of nonuniform precipitation on comparing the K_{DP} estimate using Z and Z_{DR} [*Gorgucci et al.*, 1999a, 1999b]. In this paper, the range cumulative K_{DP}, i.e., Φ^e and Φ^m, are directly compared for estimating the bias. Direct comparison of Φ_{DP} eliminates any bias introduced by nonuniform precipitation, and the least squares procedure used for estimating K_{DP}.

[24] Using the standard error results of Z, Z_{DR} and Φ_{DP} described by *Doviak and Zrnic* [1993] and the perturbation approximation, the derivation of σ_Φ is presented in Appendix A. Figure 3 shows the standard error as a function of Φ_{DP} (i.e., range) for two values of σ_v = 2.0 and 6.0 ms^{-1} for uniform precipitation. Other parameters used in the calculation are: Z_{DR} = 1dB, K_{DP} = 1° km^{-1}, number of samples N = 64, and pulse repetition frequency PRF = 1020 Hz. Figure 3a shows the standard derivations of both measured and estimated Φ_{DP}. As expected, the standard derivation of Φ^m is independent of the range whereas the standard error Φ^e increases with the range. The increase of standard deviation for the estimated Φ^e from Z and Z_{DR} is due to fluctuation error in Z and Z_{DR} that adds cumulatively. The standard deviation of estimated Φ_{DP} is lower at larger Doppler spectrum widths due to the increased number of independent samples for estimating Z and Z_{DR}. Figure 3b shows the standard error normalized by Φ_{DP} in decibel. The normalized standard errors Φ^m and Φ^e are comparable, and decrease as magnitude of Φ_m or Φ^e increases.

4. Calibration Procedure

[25] The radar data used in this study were individual ray segments having relatively long propagation paths and large Φ_{DP} values in order to minimize fluctuation in the measurements as discussed in the previous section. In order to use (9), (12) or (16) to calibrate reflectivity (Z), differential reflectivity (Z_{DR}) must be unbiased. Therefore, an independent calibration procedure for Z_{DR} is required. This is obtained by collecting precipitation data with the radar pointed vertically. In this geometry, raindrops appear spherical and will have a true average Z_{DR} of zero dB. The measured Z_{DR}, in this case, represents the system bias. The vertically pointing calibration technique is described briefly in section 4.1.

[26] It is important to avoid using radar data observations of ice particles because the calibration equations are valid only in rain. Radar artifacts, such as ground clutter echoes, overlaid second trip echoes and partial beam

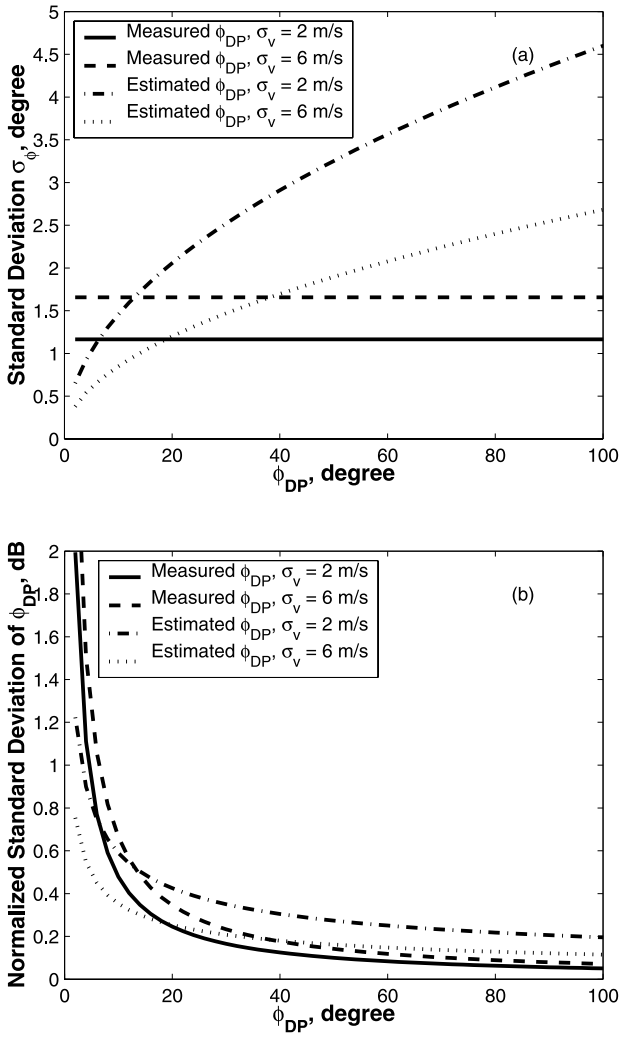

Figure 3. Standard errors of estimated and measured Φ_{DP} as a function Φ_{DP} (or range) based on perturbation analysis. (a) Standard derivations, (b) normalized standard derivations in dB.

filling must also be avoided in the data used to calibrate Z with this technique. The data quality criteria and the procedure used are described in section 4.2.

4.1. Calibration of Z_{DR}

[27] Well-calibrated Z_{DR} measurements are critical for successful reflectivity calibration because both Z and Z_{DR} are used for estimating K_{DP}, making it difficult to distinguish a bias in Z_{DR} from a bias in Z. An independent technique to calibrate Z_{DR} is readily available using data collected with the radar antenna pointing vertically. The technique takes advantage of the fact that precipitation particles have a Z_{DR} value of zero dB, on average, when viewed along the zenith, allowing a simple and accurate calibration [*Gorgucci et al.*, 1999a, 1999b].

[28] Data are collected by rotating the antenna through several complete revolutions at an elevation angle of 90°. Observations in light to moderate stratiform rain are preferred over heavy or convective rain to avoid any anisotropy due to tumbling ice particles, and mixed phase (liquid and ice) precipitation. The antenna is rotated to average any naturally occurring mean canting angle or orientation of the hydrometeors.

[29] A set of rejection criteria is applied to avoid a variety of potential errors. First, the Z_{DR} is rejected if the received power is above the saturation level of the radar receiver. Second, data with $Z < 0$ dBZ is eliminated to avoid problems associated with low signal-to-noise ratio. Last, data is rejected in the bright-band (identified using linear depolarization ratio (LDR) > -15 dB) because aggregates in the brightband may have asymmetric shapes, yielding nonzero Z_{DR} values. Figure 4 shows time-height plots of a) Z, and b) Z_{DR} with thresholds for vertical pointing data collected in a rain event in near Ji-Parana, Brazil.

[30] The Z_{DR} bias is obtained by computing the mean of the thresholded Z_{DR} measurement. Figure 4c shows a histogram of the data in Figure 4b. The bias is 0.0 dB and the standard deviation is 0.18 dB indicating a well-calibrated Z_{DR} measurement. It should be noted that the mean of the Z_{DR} measurements is computed in linear space (not dB space) to avoid the biases associated with averaging logarithms.

[31] The vertical pointing technique can only be applied when it is raining at the location of the radar, thereby constraining the frequency of the calibrations. The stability of the system can be monitored by scanning the Sun which has known measurement values. Also, a test pulse of known values can be artificially injected into the radar receiver chain and monitored for system changes. When used in combination, the vertical pointing technique, solar scans and test pulse are effective in ensuring unbiased and stable Z_{DR} measurements.

4.2. Procedure and Data Selection

[32] The calibration procedure is performed on one ray segment at a time. As discussed in section 2, Z and Z_{DR} are corrected for precipitation and gaseous attenuation. The specific differential phase (K_{DP}) is estimated from the Z and Z_{DR} measurements at each range gate and then integrated over the length of the ray to obtain an estimate for the total differential phase (Φ^e). Hence, Φ^e_{DP} is computed by integrating equation (9), (12) or (16), i.e.,

$$\Phi^e = a \int_{r_1}^{r_2} \frac{Z^b(r)}{Z^c_{DR}(r)}\, dr, \quad \text{degree} \tag{19}$$

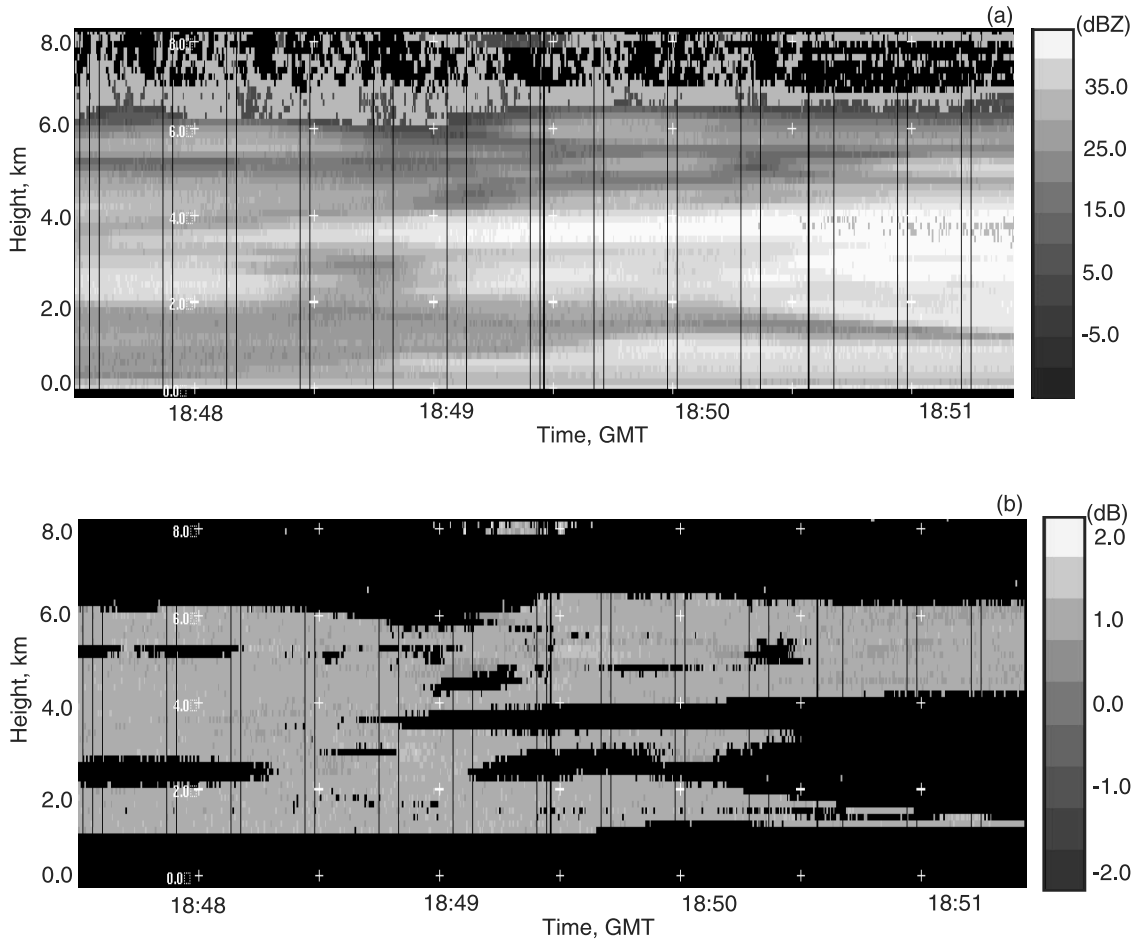

Figure 4. Time-height plots of vertical pointing radar observation. (a) Z, (b) Z_{DR} with thresholds applied and (c) histogram of Z_{DR} for the vertical pointing data shown in (b).

where r_1 and r_2 are the beginning and ending radial distance of the ray segment being considered, and a, b and c are appropriate constants from equation (9), (12), or (16).

[33] The integrals in equation (19) result in an estimate of the total measured differential phase over the length of the ray segment. The measured value of the differential phase of the ray segment, Φ^m, can be computed as the difference of the individual Φ_{DP} measurements at the beginning and end of the segment, i.e.,

$$\Phi^m = \overline{\Phi_{DP}(r_2)} - \overline{\Phi_{DP}(r_1)}, \qquad \text{(deg)} \qquad (20)$$

where $\overline{\Phi_{DP}(r_1)}$ and $\overline{\Phi_{DP}(r_2)}$ are 5 gate averages of the differential phase measurements at r_1 and r_2. The averaging is done to help alleviate measurement error. Reflectivity bias (Z_{bias}) can be estimated as,

$$Z_{bias} = 10 \log\left(\frac{\Phi^e}{\Phi^m}\right) \qquad [\text{dB}] \qquad (21)$$

[34] Since the relations used to estimate K_{DP} from Z and Z_{DR} are valid only for rain, it is necessary to avoid using beams with contamination from ice particles and ground clutter. The Hail Detection Ratio (HDR) [*Aydin et al.*, 1986] is used to discriminate liquid and ice. A value of HDR greater than 0 dB indicates the presence of ice. Due to measurement noise, a ray segment through pure liquid may contain a few radar resolution volumes with HDR > 0 dB. Therefore, if more than a predetermined number of gates (in our case 10%) within the ray exceeded the HDR limit of 0 dB, or, if the ray contained more than 4 consecutive gates with HDR > 0 dB, the beam was rejected.

[35] The calibration procedure is also not valid in the presence of radar artifacts including overlaid second trip echoes, side lobe contamination, partial beam blockage and partial beam filling. Second trip, side lobe and beam blockage contaminate the Z and Z_{DR} measurements, resulting in biased Φ^e approximations using (19) and

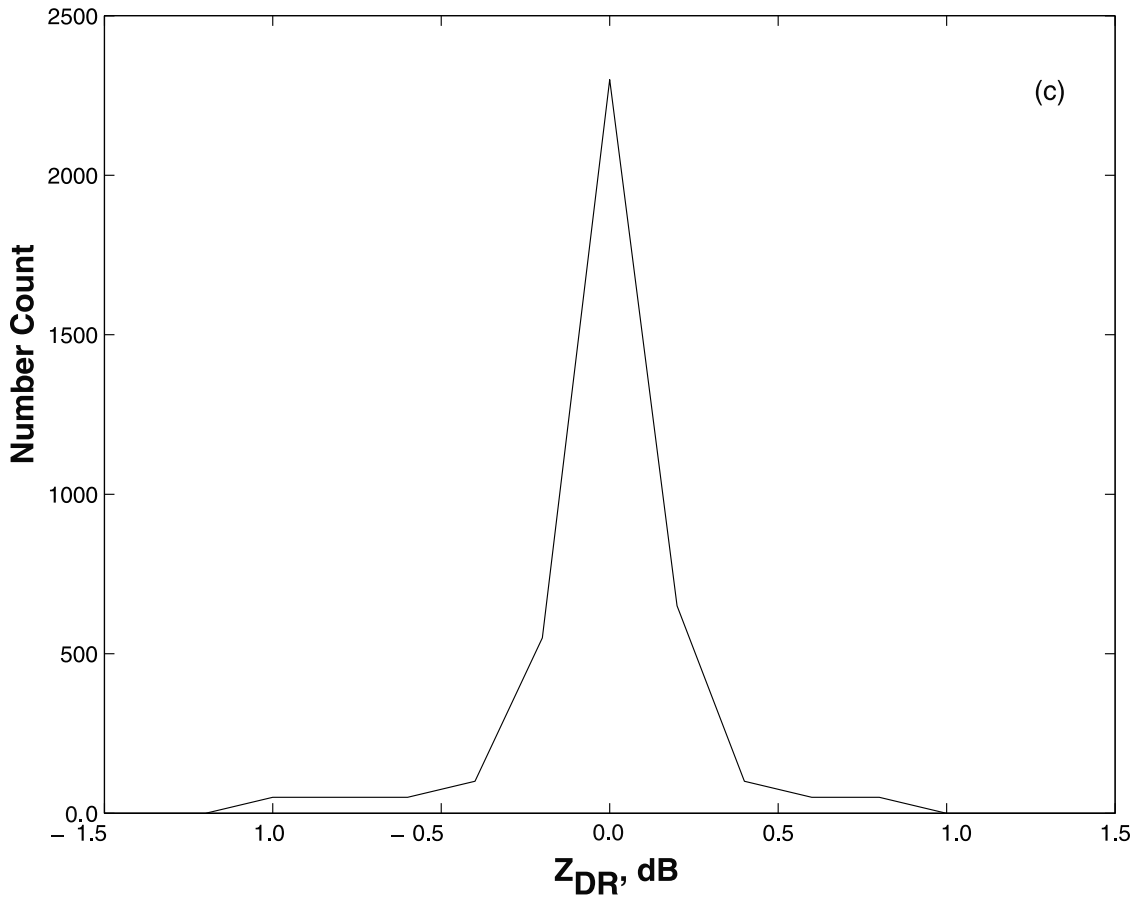

Figure 4. (continued)

(20). The Φ_{DP} measurement suffers from beam filling effects in regions of strong reflectivity gradients [*Zrnic and Ryzhkov*, 1996]. In this case, Φ_{DP} can actually decrease as the signal propagates through rain, resulting in spuriously negative K_{DP} values. The computation of Φ^e does not account for any of these radar artifacts that impact Φ^m. In order to avoid these artifacts, the data collected were carefully screened manually and longer ray segments were used.

[36] An example of polarization radar measurements of rain in Kansas during the Cooperative Atmospheric Surface Exchange Study 1997 (CASES97) experiment is presented in Figure 5; range plots of Φ_{DP}, Z, and Z_{DR} are shown. Notice the monotonically increasing values of Φ_{DP} with a two-way differential phase shift of 80° in a range of 18 km. Differential reflectivity varies between 0 and 2.5 dB, and reflectivity values are between 30 and 52 dBZ. The rain rate intensity along the beam varies between 40 and 80 mm hr^{-1}. A spectrum of polarization observations along the radial might correspond to a range of raindrop size distributions. For this particular ray, the

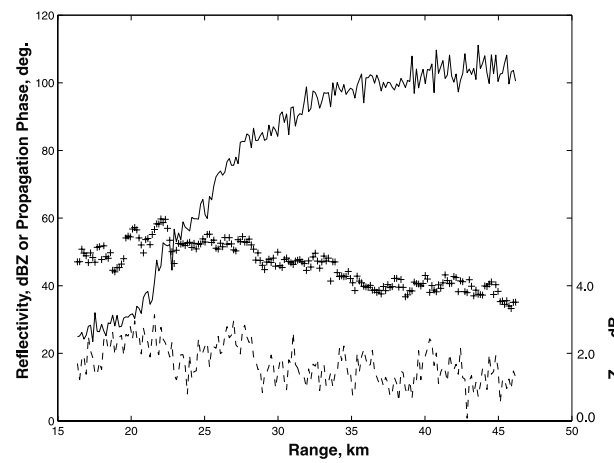

Figure 5. An example of a ray segment used in the calibration study. Plotted are Φ_{DP} in degrees (solid line), Z in dBZ (+) and Z_{DR} in dB (dashed).

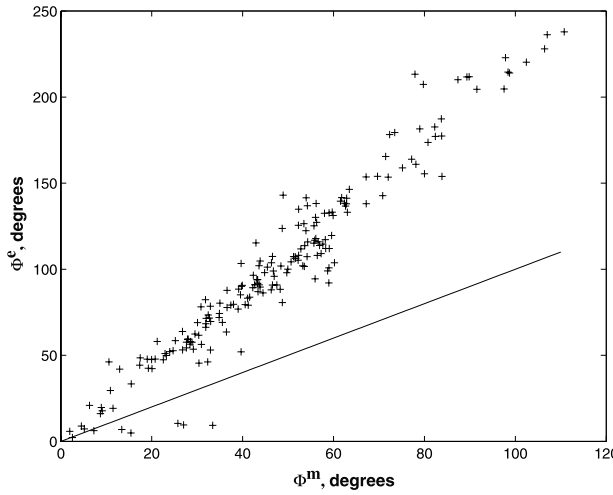

Figure 6. Analysis of radar measurements for estimating reflectivity bias. A bias of 3.29 dB in the above analysis is attributed to an error in antenna gain.

estimated and measured Φ_{DP} are 85.1° and 82.4° respectively. The resultant mean Z_{bias} is 0.14 dB for the radar measurements shown Figure 5.

[37] S-Pol data were collected from three different field campaigns: CASES97 [*Brandes et al.*, 1999] near Wichita Kansas, Precipitation 1998 (PRECIP98) near Melbourne Florida [*Brandes et al.*, 2001], and Tropical Rainfall Measuring Mission Large-Scale Biosphere-Atmosphere Experiment in Amazonia (TRMM-LBA) near Ji-Parana Brazil [*Cifelli et al.*, 2002]. The data presented below represent several days taken from each of the data sets.

5. Data Analysis

[38] Following the CASES97 field campaign, an error in the specification of the radar constant for S-Pol was discovered to have caused a bias in Z of 3.2 dB. The above described calibration procedure is applied to the polarization radar measurements in rain. The bias in radar reflectivity was also confirmed independently by comparing S-Pol and local Weather Surveillance Radar-1988 Doppler (WSR-88D) reflectivity values [*Brandes et al.*, 1999]. Figure 6 shows Φ^m versus Φ^e for a number of radar beams. The bias calculated using the polarization radar observation was 3.29 dB, in good agreement with

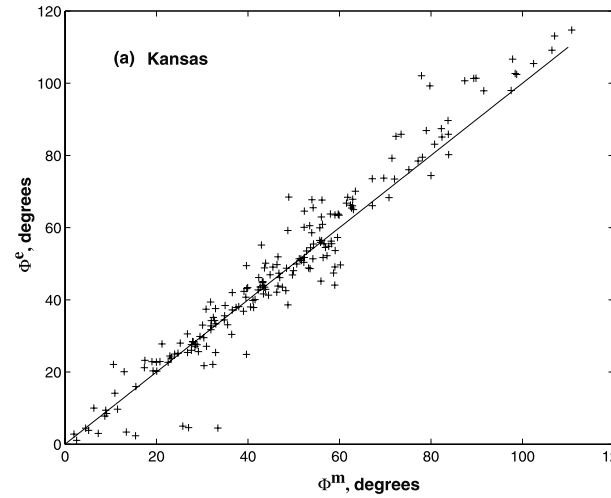

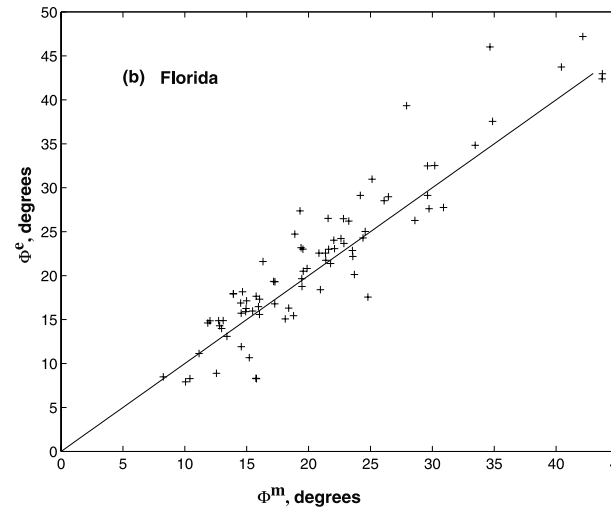

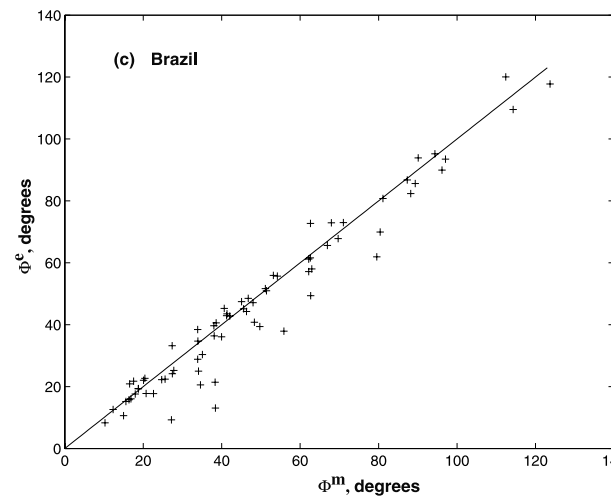

Figure 7. (opposite) Measured versus estimated Φ_{DP} for rain measurements in (a) Kansas, (b) Florida and (c) Brazil. Constrained Gamma DSD with less oblate shape is used for describing the raindrop microphysics.

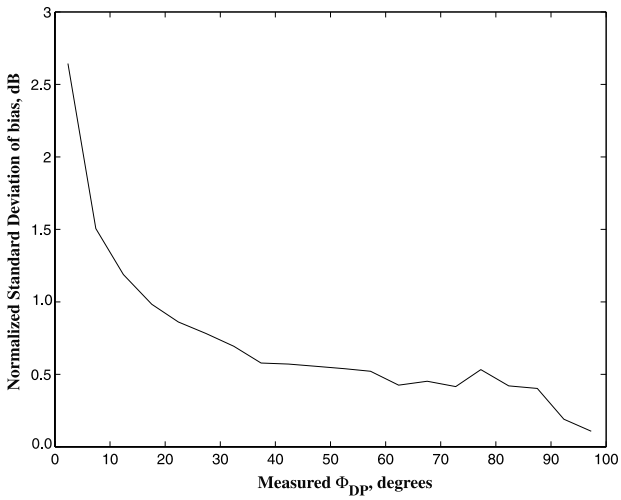

Figure 8. Measured Φ_{DP} versus normalized standard deviation in reflectivity bias. The standard deviation decreases as the propagation phase increases. The results derived from observation are in good agreement with the theoretical model shown in Figure 3b.

the known error. Detailed postanalysis of radar system parameters revealed the antenna gain was in error by 1.6 dB and the corresponding radar constant was revised. If this technique had been applied in the field, the reflectivity bias would have been detected immediately. This example shows the utility of the technique to detect bias in radar system parameters.

[39] Polarization radar measurements collected in three locations, namely Kansas (midlatitude), Florida (subtropic) and Ji Parana, Brazil (tropics), were analyzed for estimating the reflectivity bias. During all three radar deployments no changes were made to the radar system configuration. Radar engineers used solar calibrations, noise calibrations and monitored the test pulse to ensure stability of the radar system. The biases were calculated using equations (12), (16), and (19). The average propagation phase in the Brazil and Kansas data set is 50° and in the case of Florida, the spatial extent of precipitation cells is smaller and hence the corresponding mean propagation phase value is 25°. The scatterplots of two-way Φ^e versus Φ^m are presented in Figure 7 for the relation from the proposed mean raindrop shape that is less oblate than the equilibrium shape equation (19). It can be seen that the points are near the 1 to 1 line in each data set. Table 1 lists the biases for all three sets of calibration equations discussed in section 2, namely (1) Gamma DSD with equilibrium shape, (2) constrained Gamma with equilibrium shape, and (3) constrained Gamma with the proposed raindrop shape. The bias is around 1.0 dB when mean raindrop is an equilibrium shape and reduces

Table 1. Summary of Reflectivity Bias for Various Field Programs

DSD and Axis Ratio	Kansas	Brazil	Florida
Equilibrium Raindrop shape and discrete DSD	1.13	0.70	1.21
Equilibrium rain drop shape and constrained Gamma DSD	1.03	1.23	1.48
Less oblate shape and Constrained Gamma DSD	−0.23	0.10	0.20

to zero dB for the proposed raindrop shape. Variation among various data sets is less than 0.5 dB. The more spherical DSD relation yields biases near zero for all three data sets. Figure 8 shows the normalized standard deviation of Φ^e as a function of measured propagation phase. As described in section 3, the normalized standard deviation decreases as the propagation phase increases. The trend is in agreement with the simulation results shown in Figure 3b. For estimating reflectivity fluctuation within 0.5 dB, propagation phase should be larger than 40°; i.e., long rays of radar data are necessary. Typically a 20 km path in 40 mm hr^{-1} rain intensity is necessary for estimating bias within 0.5 dB.

[40] To demonstrate the importance of the attenuation correction, the above-described calibration procedure was

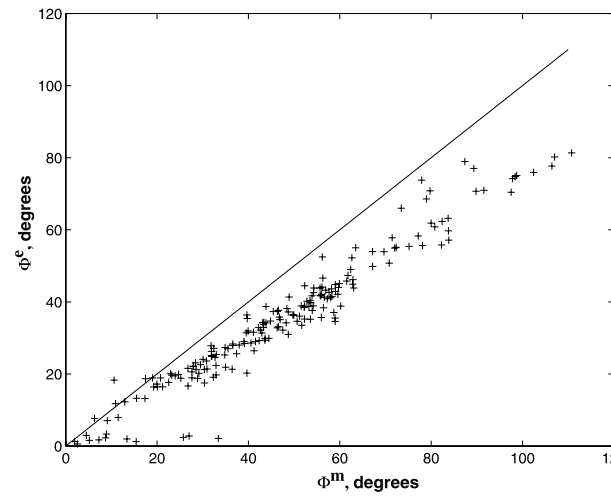

Figure 9. Measured versus estimated Φ_{DP} for rain measurements in Kansas when attenuation due to rain and gaseous absorption is neglected. A bias of −1.1 was estimated by the calibration method. Constrained Gamma DSD with less oblate shape is used for describing raindrop microphysics.

performed with no corrections applied to the Kansas data. The resulting computed bias was −1.28 dB, and the corresponding scatterplot is presented in Figure 9. The bias is negative because measured reflectivity is reduced by attenuation. Thus it is important to account for attenuation to obtain a reflectivity bias within one dB.

6. Conclusions

[41] A technique for calibrating radar reflectivity using polarization radar measurements in rain is described. Since the polarization observations are sensitive to DSD and mean raindrop shape, various calibration equations are derived using model calculations. A two parameter Gamma DSD based on μ-Λ relation and three parameter discrete DSD produced almost similar reflectivity bias results. Thus the closed-form calibration equation can be used instead of intensive model calculation based on discrete DSD. The calibration equation is analyzed for change in drop shape. The calibration equation based on a less oblate raindrop shape shows almost no bias in radar reflectivity in all three field programs. A detailed comparison between rain gauge and radar estimated rain in Kansas and Florida also suggests no bias in reflectivity [*Brandes et al.*, 1999, 2001]. In the case of Brazil, no independent verification of reflectivity bias is performed. However, other auxiliary calibration methods using noise diode and solar calibration showed there is no significant change in absolute calibration of the radar system. NCAR is in the process of implementing the calibration procedure described in this paper for real-time application.

Appendix A

[42] As shown in the text, K_{DP} can be estimated from Z and Z_{DR} measurements as

$$K_{DP} = c\, Z^{\alpha} Z_{DR}^{\beta}. \tag{A1}$$

[43] Fluctuation and mean components of Z and Z_{DR} can be expressed as

$$Z = \langle Z \rangle + \Delta Z \tag{A2a}$$

$$Z_{DR} = \langle Z_{DR} \rangle + \Delta Z_{DR}. \tag{A2b}$$

Substituting (A2) in (A1), and taking an ensemble average, we have

$$\begin{aligned}\langle K_{DP} \rangle &= c(\langle Z \rangle + \Delta Z)^{\alpha}(\langle Z_{DR} \rangle + \Delta Z_{DR})^{\beta} \\ &= c\langle Z \rangle^{\alpha}\langle Z_{DR} \rangle^{\beta}\left(1 + \frac{1}{2}\alpha(\alpha-1)\frac{\sigma_Z^2}{\langle Z \rangle^2}\right. \\ &\quad \left. + \frac{1}{2}\beta(\beta-1)\frac{\sigma_{Z_{DR}}^2}{\langle Z_{DR} \rangle^2} + \alpha\beta\frac{\rho_{Z,Z_{DR}}}{\langle Z \rangle\langle Z_{DR} \rangle}\right).\end{aligned} \tag{A3}$$

[44] Similarly, we obtain

$$\begin{aligned}\langle K_{DP}^2 \rangle &= \left\langle c^2(\langle Z \rangle + \Delta Z)^{2\alpha}(\langle Z_{DR} \rangle + \Delta Z_{DR})\right\rangle \\ &\approx c^2\langle Z \rangle^{2\alpha}\langle Z_{DR} \rangle^{2\beta}\left(1 + \alpha(\alpha-1)\frac{\sigma_Z^2}{\langle Z \rangle^2}\right. \\ &\quad \left. + \beta(\beta-1)\frac{\sigma_{Z_{DR}}^2}{\langle Z_{DR} \rangle^2} + 4\alpha\beta\frac{\rho_{Z,Z_{DR}}}{\langle Z \rangle\langle Z_{DR} \rangle}\right)\end{aligned} \tag{A4}$$

[45] Subtracting a square of (A3) from (A4) yields

$$\begin{aligned}\sigma_{K_{DP}}^2 &= \langle K_{DP}^2 \rangle - \langle K_{DP} \rangle^2 \\ &= c^2\langle Z \rangle^{2\alpha}\langle Z_{DR} \rangle^{2\beta}\left(\alpha^2\frac{\sigma_{Z_{DR}}^2}{\langle Z \rangle^2} + \beta^2\frac{\rho_{Z,Z_{DR}}}{\langle Z_{DR} \rangle^2}\right. \\ &\quad \left. + 2\alpha\beta\frac{\rho_{Z,Z_{DR}}}{\langle Z \rangle\langle Z_{DR} \rangle}\right).\end{aligned} \tag{A5}$$

[46] Differential propagation phase Φ_{DP} over a range L is

$$\begin{aligned}\Phi_{DP} &= 2\int_0^L K_{DP}(l)dl \\ \langle \Phi_{DP} \rangle &\approx 2\langle K_{DP} \rangle L.\end{aligned} \tag{A6}$$

$$\begin{aligned}\langle \Phi_{DP}^2 \rangle &= \left\langle \left[2\int_0^L K_{DP}(l)dl\right]^2 \right\rangle \\ &= 4\left\langle \int_0^L K_{DP}(l)dl \int_0^L K_{DP}(l')dl' \right\rangle \\ &= 4\left\langle \int_0^L \langle\langle K_{DP}(l)\rangle + \Delta K_{DP}(l)\rangle dl \int_0^L (\langle K_{DP}(l')\rangle \right. \\ &\quad \left. + \Delta K_{DP}(l'))dl' \right\rangle \\ &\approx 4\langle K_{DP} \rangle^2 L^2 + 4Ll_c\sigma_{K_{DP}}^2\end{aligned} \tag{A7}$$

l_c is the range gate width

$$\begin{aligned}\sigma_{\Phi_{DP}}^2 &= \langle \Phi_{DP}^2 \rangle - \langle \Phi_{DP} \rangle^2 \\ &= 4Ll_c\sigma_{K_{DP}}^2\end{aligned} \tag{A8}$$

Using equations (A5) and (A8) and the results of standard deviation of Z, Z_{DR}, the standard error in Φ_{DP} is found.

[47] **Acknowledgments.** The research is sponsored by the National Science Foundation through an Interagency Agreement in response to requirements and funding by the Federal Aviation Administration's Aviation Weather Development Program. Robert Rilling of NCAR produced Figures 4a and 4b.

The authors would like to thank J. S. Lutz, M. A. Randall, and D. A. Ferraro for the excellent performance of S-Pol radar, and also thanks to radar operators A. D. Phiney, T. D. Rucker, M. A. Strong, and J. P. Vinson. In addition, they would like to thank Robert Rilling and Jean Hurst for preparing radar tapes for analysis and R. Oye for software support.

References

Andsager, K., K. V. Beard, and N. F. Laird, Laboratory measurements of axis ratios for large drops, *J. Atmos. Sci..*, *56*, 2673–2683, 1999.

Aydin, K., T. A. Seliga, and V. Balaji, Remote sensing of hail with a dual-linear polarization radar, *J. Clim. Appl. Meteorol.*, *25*, 1475–1484, 1986.

Beard, K. V., and C. Chuang, A new model for the equilibrium shape of raindrops, *J. Atmos. Sci.*, *44*, 1509–1524, 1987.

Beard, K. V., and R. J. Kubesh, Laboratory measurements of small raindrop distortion, 2, Oscillations, *J. Atmos. Sci.*, *48*, 2245–2264, 1991.

Brandes, E. A., J. Vivekanandan, and J. W. Wilson, Comparison of radar reflectivity: Estimates from collocated radars, *J. Atmos. Oceanic Technol.*, *16*, 1264–1272, 1999.

Brandes, E. A., G. Zhang, and J. Vivekanandan, Experiments in rainfall estimation with a polarimetric radar in a subtropical environment, *J. Appl. Meteorol.*, *41*, 674–685, 2001.

Bringi, V. N., and A. Hendry, Technology of polarization diversity radars of meteorology, in *Radar in Meteorology*, pp. 153–190, Am. Meteorol. Soc., Boston, Mass., 1990.

Bringi, V. N., V. Chandrasekar, N. Balakrishnan, and D. S. Zrnic, An examination of propagation effects in rainfall on radar measurements at microwave frequencies, *J. Atmos. Oceanic Technol.*, *7*, 829–840, 1990.

Bringi, V. N., V. Chandrasekar, and R. Xiao, Raindrop axis ratios and size distributions in Florida rainshafts: An assessment of multiparameter radar algorithm, *IEEE Trans. Geosci. Remote Sens.*, *36*, 703–715, 1998.

Chandrasekar, V. V., and V. N. Bringi, Simulation of radar reflectivity and surface measurements of rainfall, *J. Atmos. Oceanic Technol.*, *4*, 464–478, 1987.

Chandrasekar, V., A. Cooper, and V. N. Bringi, Axis ratios and oscillations of raindrops, *J. Atmos. Sci.*, *45*, 1323–1333, 1988.

Cifelli, R., W. A. Petersen, L. D. Carey, S. A. Rutledge, and M. A. F. Silva Dias, Radar observations of the kinematic, microphysical, and precipitation characteristics of two MCSs in TRMM LBA, *J. Geophys. Res.*, *107*(D20), 8077, doi:10.1029/2000JD000264, 2002.

Doviak, J. D., and D. S. Zrnic, *Doppler Radar and Weather Observations*, 2nd ed., Academic, San Diego, Calif., 1993.

Goddard, J. W. F., and S. M. Cherry, The ability of dual-polarized radar (copolar linear) to predict rainfall rate and microwave attenuation, *Radio Sci.*, *19*, 201–208, 1984.

Goddard, J. W. F., J. Tan, and M. Thurai, Technique for calibration of meteorological radars using differential phase, *Electron. Lett.*, *30*, 166–167, 1994.

Gorgucci, E., G. Scarchilli, and V. Chandrasekar, Calibration of radars using polarimetric techniques, *IEEE Trans. Geosci. Remote Sens.*, *30*, 853–858, 1992.

Gorgucci, E., G. Scarchilli, and V. Chandrasekar, A robust estimator of rainfall rate using differential reflectvity, *J. Atmos. Oceanic Technol.*, *11*, 586–592, 1993.

Gorgucci, E., G. Scarchilli, and V. Chandrasekar, Specific differential phase estimation in the presence of nonuniform rainfall medium along the path, *J. Appl. Meteorol.*, *34*, 1690–1697, 1999a.

Gorgucci, E., G. Scarchilli, and V. Chandrasekar, A procedure to calibrate multiparameter weather radar using properties of the rain medium, *IEEE Trans. Geosci. Remote Sens.*, *37*, 269–276, 1999b.

Green, A. W., An approximation for shapes of large drops, *J. Appl. Meteorol.*, *14*, 1578–1583, 1975.

Haddad, Z. S., D. A. Short, S. L. Durden, E. Im, S. Hensley, M. B. Grable, and R. A. Black, A new parameterizing of raindrop size distribution, *IEEE Trans. Geosci. Remote Sens.*, *35*, 532–539, 1997.

Illingworth, A. J., and T. M. Blackman, The need to normalize RSDs based on the Gamma RSD formulations and implications for interpreting polarimetric radar data, in *29th International Conference On Radar Meteorology*, pp. 629–631, Am. Meteorol. Soc., Boston, Mass., 1999.

Jameson, A. R., Microphysical interpretation of multiparameter radar measurements in rain, 1, Interpretation of polarization measurements and estimation of raindrop shapes, *J. Atmos. Sci.*, *40*, 1792–1802, 1983a.

Jameson, A. R., Microphysical interpretation of multiparameter radar measurements in rain, 2, Estimation of raindrop distribution parameters by combined dual-wavelength and polarization measurements, *J. Atmos. Sci.*, *40*, 1803–1813, 1983b.

Jameson, A. R., and E. A. Mueller, Estimation of propagation-differential phase shift from sequential orthogonal linear polarization radar measurements, *J. Atmos. Oceanic Technol.*, *2*, 133–137, 1985.

McCormick, G. C., and A. Hendry, Principles for the determination of the polarization properties of precipitation, *Radio Sci.*, *10*, 421–434, 1975.

Oguchi, T., Electromagnetic wave propagation and scattering in rain and other hydrometeors, *Proc. IEEE*, *71*, 1029–1079, 1983.

Pruppacher, H. R., and R. L. Pitter, A semi-empirical determination of the shape of cloud and raindrops, *J. Atmos. Sci.*, *28*, 86–94, 1971.

Scarchilli, G., E. Gorgucci, V. Chandrasekar, and A. Dobaie, Self consistency of polarization diversity measurements of rainfall, *IEEE Trans. Geosci. Remote Sens.*, *34*, 22–26, 1996.

Schonhuber, M., H. E. Urban, J. P. V. P. Baptista, W. L. Randeu, and W. Riedler, Weather radar versus 2D-video disdrometer data, in *Weather Radar Technology for Water Resources Management*, edited by B. Braga Jr. and O. Massambani, pp. 159–171, UNESCO Press, Montevideo, Uruguay, 1997.

Testud, J., S. Oury, R. A. Black, P. Amayenc, and X. Dou, The concept of "normalized" distributions to describe raindrop spectra: A tool for cloud physics and cloud remote sensing, *J. Appl. Meteorol.*, *40*, 1118–1140, 2001.

Ulbrich, C. W., Natural variations in the analytical form of the raindrop size distribution, *J. Clim. Appl. Meteorol.*, *22*, 1764–1775, 1983.

Vivekanandan, J., W. M. Adams, and V. N. Bringi, Rigorous approach to polarimetric radar modeling of hydrometeor orientation distributions, *J. Appl. Meteorol.*, *30*, 1053–1063, 1991.

Vivekanandan, J., D. N. Yates, and E. A. Brandes, The influence of terrain on rainfall estimations from radar reflectivity and specific propagation phase observations, *J. Atmos. Oceanic Technol.*, *16*, 837–845, 1999.

Willis, P. T., Functional fits to some observed drop size distributions and parameterization of rain, *J. Atmos. Sci.*, *41*, 1648–1661, 1984.

Zhang, G., J. Vivekanandan, and E. Brandes, A method for estimating rain rate and drop size distribution from polarimetric radar measurements, *IEEE Trans. Geosci. Remote Sens.*, *39*, 830–841, 2001.

Zrnic, D. S., and A. Ryzhkov, Advantages of rain measurements using specific differential phase, *J. Atmos. Oceanic Technol.*, *13*, 454–464, 1996.

S. K. Avery and D. Rajopadhyaya, Cooperative Institute for Research in Environmental Sciences, University of Colorado, Boulder, CO 80309, USA.

S. M. Ellis, J. Vivekanandan, and G. Zhang, National Center for Atmospheric Research, P.O. Box 3000, Boulder, CO 80307, USA. (vivek@ucar.edu)